BJP British Journal of Pharmacology

DOI:10.1111/bph.12846
www.brjpharmacol.org

RESEARCH PAPER

Metabolic characteristics of 13-cis-retinoic acid (isotretinoin) and anti-tumour activity of the 13-cis-retinoic acid metabolite 4-oxo-13-cis-retinoic acid in neuroblastoma

Poonam Sonawane[1,2], Hwang Eui Cho[1,2], Ashujit Tagde[1,2], Dattesh Verlekar[1,2], Alice L Yu[3,4], C Patrick Reynolds[1,2,5] and Min H Kang[1,2,5]

[1]*Cancer Center, Texas Tech University Health Sciences Center, Lubbock, TX, USA,* [2]*Pharmacology and Neuroscience, Texas Tech University Health Sciences Center, Lubbock, TX, USA,* [3]*Department of Pediatrics, University of California, San Diego, CA, USA,* [4]*Institute of Stem Cell & Translational Cancer Research, Chang Gung Memorial Hospital, Taoyuan, Taiwan, and* [5]*Cell Biology and Biochemistry, School of Medicine, Texas Tech University Health Sciences Center, Lubbock, TX, USA*

Correspondence
Min H Kang, School of Medicine, Texas Tech University Health Sciences Center, 3601 4th Street, Mail Stop 6540, Lubbock, TX 79430, USA. E-mail: min.kang@ttuhsc.edu

Received
6 January 2014
Revised
4 July 2014
Accepted
8 July 2014

BACKGROUND AND PURPOSE

Isotretinoin (13-cis-retinoic acid; 13-cRA) is a differentiation inducer used to treat minimal residual disease after myeloablative therapy for high-risk neuroblastoma. However, more than 40% of children develop recurrent disease during or after 13-cRA treatment. The plasma concentrations of 13-cRA in earlier studies were considered subtherapeutic while 4-oxo-13-cis-RA (4-oxo-13-cRA), a metabolite of 13-cRA considered by some investigators as inactive, were greater than threefold higher than 13-cRA. We sought to define the metabolic pathways of 13-cRA and investigated the anti-tumour activity of its major metabolite, 4-oxo-13-cRA.

EXPERIMENTAL APPROACH

Effects of 13-cRA and 4-oxo-13-cRA on human neuroblastoma cell lines were assessed by DIMSCAN and flow cytometry for cell proliferation, MYCN down-regulation by reverse transcription PCR and immunoblotting, and neurite outgrowth by confocal microscopy. 13-cRA metabolism was determined using tandem MS in human liver microsomes and in patient samples.

KEY RESULTS

Six major metabolites of 13-cRA were identified in patient samples. Of these, 4-oxo-13-cRA was the most abundant, and 4-oxo-13-cRA glucuronide was also detected at a higher level in patients. CYP3A4 was shown to play a major role in catalysing 13-cRA to 4-oxo-13-cRA. In human neuroblastoma cell lines, 4-oxo-13-cRA and 13-cRA were equi-effective at inducing neurite outgrowth, inhibiting proliferation, decreasing *MYCN* mRNA and protein, and increasing the expression of retinoic acid receptor-β mRNA and protein levels.

CONCLUSIONS AND IMPLICATIONS

We showed that 4-oxo-13-cRA is as active as 13-cRA against neuroblastoma cell lines. Plasma levels of both 13-cRA and 4-oxo-13-cRA should be evaluated in pharmacokinetic studies of isotretinoin in neuroblastoma.

Abbreviations

13-cRA, 13-cis-retinoic acid; 4-oxo-13-cRA, 4-oxo-13-cis-retinoic acid; ASCT, autologous haematopoietic stem cell transplantation; ATRA, all-trans-retinoic acid; CCG, Children's Cancer Group; COG, Children's Oncology Group; CYP, cytochrome P450; HIM, human intestinal microsomes; HLM, human liver microsomes; NB, neuroblastoma; RT-PCR, reverse transcription PCR

Table of Links

TARGETS	LIGANDS
CYP2B6	All-trans-retinoic acid
CYP2C8	Gemfibrozil
CYP2C9	Ketoconazole
CYP2C19	NADPH
CYP3A4	Uridine diphosphoglucuronic acid
CYP3A5	
IGF1R	
Oestrogen receptor-α	
PPAR	
RARβ	

This Table lists key protein targets and ligands in this document, which are hyperlinked to corresponding entries in http://www.guidetopharmacology.org, the common portal for data from the IUPHAR/BPS Guide to PHARMACOLOGY (Pawson *et al.*, 2014) and are permanently archived in the Concise Guide to PHARMACOLOGY 2013/14 (Alexander *et al.*, 2013a,b).

Introduction

Neuroblastoma (NB) is a cancer of the sympathetic nervous system and one of the most common childhood cancers that has approximately 650 new cases per year (Maris and Matthay, 1999; Maris *et al.*, 2007). High-risk patients are those patients >18 months old with stage 4 disease, stage 3 tumours with unfavourable histopathology, or any tumour with v-myc avian myelocytomatosis viral-related oncogene, neuroblastoma-derived (*MYCN)* gene amplification (Maris and Matthay, 1999; London *et al.*, 2011). Nearly 50% of patients present with metastatic disease and have a 5 year event-free survival (EFS) of <50%. Treatment of high-risk NB with non-myeloablative (conventional) chemotherapy achieves an initial response in most patients, but eventually 80–90% of high-risk patients treated with only conventional chemotherapy develop progressive disease, which is refractory to further therapy (Matthay *et al.*, 1995; 1999). The Children's Oncology Group (COG) has shown that, after induction therapy, consolidation of responding patients with intensive multi-agent therapy supported by autologous haematopoietic stem cell transplantation (ASCT) improved outcome from ~30 to 50% for high-risk NB (Matthay *et al.*, 1999; 2009; Kreissman *et al.*, 2013), especially if patients receive post-ASCT maintenance therapy with 13-cis-retinoic acid (13-cRA; Matthay *et al.*, 1999) + ch14.18 antibody and cytokines (Yu *et al.*, 2010). Although the effect of immunotherapy on long-term survival remains to be determined, approximately 50% of high-risk NB patients ultimately die from the disease, either from progression before ASCT or (the majority) from relapse after ASCT and maintenance therapy (Matthay *et al.*, 1999; 2009; Yu *et al.*, 2010; Kreissman *et al.*, 2013; Park *et al.*, 2013).

NB can spontaneously mature to a benign tumour known as ganglioneuroma (Abemayor and Sidell, 1989; Iwanaka *et al.*, 2001). These clinical observations have stimulated studies of NB differentiation *in vitro*. A variety of agents have been shown to induce growth arrest and neurite outgrowth of human NB cell lines, and one of the most potent differentiation inducers is all-trans-retinoic acid (Haussler *et al.*, 1983; Sidell *et al.*, 1983). Treatment of both *MYCN* gene-amplified and non-amplified human NB cells with retinoic acid caused a marked decrease in *MYCN* mRNA expression and arrest of cell proliferation (Sidell, 1982; Haussler *et al.*, 1983; Thiele *et al.*, 1985; Li *et al.*, 1994). Previous reports showed that 5 μM 13-cRA given in 2 week pulse treatments can achieve long-term growth arrest of NB cell lines *in vitro* (Reynolds *et al.*, 2003). These data and the favourable pharmacokinetics of 13-cRA compared with all-trans-retinoic acid (ATRA) prompted the use of high-dose, pulse 13-cRA rather than

ATRA for clinical studies in NB patients, which showed anti-NB activity of 13-cRA, even in patients who had residual or progressive disease after cytotoxic therapy (Greenberg *et al.*, 1985; Reynolds *et al.*, 1991; 2003; Seeger and Reynolds, 1991; Finklestein *et al.*, 1992; Villablanca *et al.*, 1995). A nationwide phase III study with the Children's Cancer Group (CCG-3891) proving effectiveness for high-dose, pulse 13-cRA in preventing relapse from minimal residual disease resulted in post-consolidation therapy with 13-cRA becoming a worldwide standard of care for high-risk NB (Matthay *et al.*, 1999), recently in combination with the ch14.18 anti-GD2 antibody and cytokines (Yu *et al.*, 2010).

In vitro studies showed that a minimum of 5 μM 13-cRA was required for sustained neurite outgrowth, cell cycle arrest and a sustained decreased expression of the *MYCN* oncogene in NB cell lines (Reynolds *et al.*, 1994). However, clinical studies with 13-cRA reported much higher accumulation of the phase I oxidation metabolite 4-oxo-13-cis-retinoic acid (4-oxo-13-cRA; mean plasma levels: 3.5–6.4 μM on day 14 of course 2–6) than 13-cRA in the majority of patients, with 13-cRA levels being much lower than what is considered therapeutic (Khan *et al.*, 1996; Veal *et al.*, 2007). The low plasma levels of 13-cRA apparently being achieved were not consistent with the demonstrated increase in event-free survival achieved in patients randomized to 13-cRA versus no further therapy (Matthay *et al.*, 1999; 2009; Park *et al.*, 2009), suggesting that 4-oxo-13-cRA might be an active metabolite.

We hypothesized that 4-oxo-13-cRA is equally as active as 13-cRA in NB and achieving high plasma concentrations of either 13-cRA or 4-oxo-13-cRA are critical to the therapeutic benefit observed in NB. In the current study, we defined the metabolic pathways of 13-cRA, using human liver microsomes (HLM), hepatocytes, mice and patient samples, and determined the ability of 4-oxo-13-cRA in comparison with 13-cRA to induce morphological differentiation, arrest of cell proliferation and down-regulation of *MYCN* expression.

Methods

Cell lines and culture conditions

We used seven human NB cell lines established from six different patients, including four *MYCN*-amplified cell lines SMS-KCNR, SMS-KCN, SMS-KANR and SK-N-BE(2) and three *MYCN* non-amplified cell lines CHLA-79, CHLA-20 and SMS-LHN (Keshelava *et al.*, 1998). Cell lines were obtained from the COG Cell Culture Repository (http://www.COGcell.org). CHLA-79 and CHLA-20 cells were cultured in complete medium consisting of Iscove's Modified Dulbecco's Medium (Cambrex, East Rutherford, NJ, USA) supplemented with 3 mM L-glutamine, 5 mg·mL^{-1} insulin and 20% heat-inactivated FBS. The other cell lines were maintained in RPMI-1640 (Mediatech Inc., Manassas, VA, USA) supplemented with 10% heat-inactivated FBS. All cell lines were tested in mycoplasma-free media and were maintained at 37°C in humidified incubators containing 95% air + 5% CO_2 atmosphere. Cell line identities were confirmed at the time of experimentation by short tandem repeat (STR) genotyping as previously described (Masters *et al.*, 2001) and compared with the COG STR database (http://www.COGcell.org).

Measuring retinoic acid-induced growth inhibition

To compare the growth inhibition between 13-cRA and 4-oxo-13-cRA, DIMSCAN, a semiautomatic fluorescence-based digital image microscopy system (DIMSCAN), was used (Frgala *et al.*, 2007). Cells were incubated in the presence of drug for 10 days with the medium containing drug replenished on day 5. Mean fluorescence values were determined for each concentration tested and then normalized to the mean control fluorescence. A non-linear regression, sigmoidal dose–response model was fitted using GraphPad Prism (GraphPad Software, La Jolla, CA, USA) 5.03 to the relative mean fluorescence values versus the log-transformed concentration for the calculation of relative 50% inhibitory concentrations (rIC_{50}; Kang *et al.*, 2010).

Real-time reverse transcription PCR (RT-PCR)

Gene expression of the following genes was measured by real-time RT-PCR using Applied Biosystems (Framingham, MA, USA) Prism 7900HT: *MYCN*, retinoic acid receptor-β (*RAR-β isoforms 1, 2, 3, 4, 5, 7, 8*), cytochrome P450 (CYP), family 3, subfamily A, polypeptide 4 (*CYP3A4*), CYP, family 3, subfamily A, polypeptide 4 (*CYP3A5*), CYP, family 2, subfamily C, polypeptide 9 (*CYP2C9*), CYP, family 2, subfamily C, polypeptide 19 (*CYP2C19*), CYP, family 2, subfamily B, Polypeptide 6 (*CYP2B6*) and CYP, family 2, subfamily C, polypeptide 8 (*CYP2C8*). The reagents, assay conditions and data normalization methods were as previously described (Kang *et al.*, 2008). RNA was extracted from cells treated with 5 μM 13-cRA, 4-oxo-13-cRA or vehicle control using Qiagen RNA extraction kit (Valencia, CA, USA). The RT-PCR assays were conducted in 96-well plates in triplicates using TaqMan one-step RT-PCR Master Mix Reagents (Applied Biosystems), 200 nM of forward and reverse primers, 100 nM probe, and 100 ng of total RNA in a total volume of 25 μL. Gene expression was normalized by GAPDH and 18S mRNA levels. The primers and probes used for the experiments are listed in Supporting Information Table S1.

Immunoblot analysis

Treated and control cells were harvested and the cell pellets were washed twice with ice-cold PBS. Briefly, the cells were lysed in RIPA lysis buffer (1X PBS, 1% NP-40, 1% sodium deoxycholate and 0.1 % SDS) with protease inhibitor (0.3M) and phosphatase inhibitor cocktail (1X) (both reagents from Cell Signaling, Beverly, MA, USA) on ice for 30 min. After centrifugation for 30 min at 14 000× *g*, the supernatant protein lysates were collected. Protein concentrations were measured using the Bicinchoninic Acid Protein Assay (Thermo Scientific, Waltham, MA, USA). After being denatured, protein samples were separated on NuPage Novex 4–12% Bis-Tris precast gels (Invitrogen, Carlsbad, CA, USA) and transferred to PVDF membrane (Protran, Pittsburgh, PA, USA) and probed with antibodies for RAR-β, MYCN, NeuN, MAP-2c, vimentin or β-actin (for a loading control) from Santa Cruz Biotechnology. Visualization of the protein bands was done using HRP-conjugated secondary antibody and ECL detection kit (Amersham, Pittsburgh, PA, USA).

Cell proliferation by flow cytometry

Effect of 13-cRA and 4-oxo-13-cRA treatment on cell proliferation was determined by examining the distribution of cells

in different phases of the cell cycle by flow cytometry. Cells were incubated with 13-cRA or 4-oxo-13-cRA (5 μM) for 10 days, with the complete medium and the drugs being replaced every 96 h. Cells were harvested and incubated with 40 μg·mL^{-1} RNase A for 30 min at 37°C. Pelleted cells were stained with 40 μg·mL^{-1} PI and flow cytometric analysis was performed using a BD LSR II flow cytometer (BD Biosciences, San Jose, CA, USA), which was operated with DiVA (version 4.1.2) software (BD Biosciences). PI was detected in the 610/20 nm channel and the cell flow rate was set at 100 events·s^{-1}. Data obtained by flow cytometry were analysed using FlowJo software (Three Star Inc., Ashland, OR, USA).

Neurite outgrowth by confocal microscopy

Cells were seeded on glass coverslips in 6-well plates and treated with either 13-cRA, 4-oxo-13-cRA or vehicle, three conditions per cell line (SMS-KCNR, SMS-LHN) for 10 days. At the end of the 10th day, cells were fixed with 1 mL of 4% paraformaldehyde and permeabilized in 0.2% BSA-PBS 1X containing 0.1% Triton X-100, then blocked with 2% BSA in 1X PBS for 30 min and probed with Alexa Fluor 488 phalloidin (1:100) (Invitrogen), followed by DAPI. Images were obtained using Nikon confocal microscope (NIS-Elements AR 3.2, Nikon, Melville, NY, USA) with a ×60 objective (Plan Apo VC, 1.4 numerical aperture (NA), oil differential interference contrast). Images of Alexa fluor 488 phalloidin (actin cytoskeleton) fluorescence were collected, and each image was analysed and converted to TIFF by use of an Olympus (Center Valley, PA, USA) IX-71 inverted microscope with a 60x/1.4 NA objective lens. A 430–460 barrier filter was used to detect the DAPI, and a 510 barrier filter was used to detect the phalloidin for analysis of fluorescence intensity; neurite length was measured using MetaMorph software (Molecular Devices, Sunnyvale, CA, USA).

Identification of 13-cRA metabolites in patient samples using tandem MS

Twenty-seven patients whose plasma samples were used for metabolite identification were enrolled in a COG phase III study (COG ANBL0032; Yu *et al.*, 2010). Four hours after the morning dose (160 mg·m^{-2}·day^{-1}) of 13-cRA on day 14, 5 mL of blood was collected in a foil-wrapped heparin-treated tube, centrifuged immediately and plasma was collected for analysis. All procedures were carried out in amber tubes under recessed yellow lighting. The patients gave written informed consent and the study received Institutional Review Board approval in participating institutions.

Identification of metabolites was done using LC/MS/MS. An Agilent (Agilent Technologies, Santa Clara, CA, USA) 1200 HPLC was used with an Applied Biosystems 4000 QTRAP MS/MS, and the MS/MS was operated in electrospray positive ion mode for analysis. For preparation of samples, 300 μL of ice-cold methanol was added to 100 μL of patient plasma, vortexed (1 min), and centrifuged at 10 000× *g* for 5 min. Samples were evaporated and reconstituted as described above; 10 μL of the reconstituted sample was injected into the LC/MS/MS. A C18 column 150 × 3 mm, 3.0 μm Zorbax column (Agilent Technologies) was used for separation. The mobile phase used was 2 mM ammonium formate and water with 0.1% formic acid; 1 mM ammonium formate in methanol with 0.1% formic acid with a flow rate of 0.300 mL·min^{-1}. The system was operated in an information-dependent acquisition (IDA) mode (threshold: 1000 cps), which was set to include an MS3 experiment following an enhanced product ion spectrum for the parent ion in transition. Data processing and acquisition were done using Analyst (AB Sciex, Framingham, MA, USA, version 1.4.2) and LightSight Metabolite ID software (AB Sciex).

Animals

Twelve mice, 6–7-weeks-old BALB/c were obtained from Charles River Laboratories International (Wilmington, MA, USA). The animals were housed in a controlled environment (21 ± 2°C and 40-60% relative humidity) and provided with standard rodent pelleted chow and water. Animals were allowed to acclimatize for 7 days before the experiments and were subjected to a diurnal 12 h light cycle. Experiments were conducted during the light phase. The treatment group received 13-cRA formulated in corn oil and the control group received vehicle via gavage, the exact doses of 13-cRA are given in the figure legend. The mice were divided into three groups, each group consisting of four mice, day 1, day 3 and day 5. One of the four mice was control and the remaining three were the mice receiving 13-cRA treatment. All mice were housed, treated and killed according to protocols approved by the TTUHSC Institutional Animal Care and Use Committee, and all studies involving animals are reported in accordance with the ARRIVE guidelines for reporting experiments involving animals (Kilkenny *et al.*, 2010; McGrath *et al.*, 2010).

HPLC analysis

We measured the levels of 13-cRA, 4-oxo-13-cRA and ATRA using HPLC (Agilent 1200 HPLC system). The HPLC method used a C18 column from Agilent Zorbax Eclipse, 150 × 4.6 mm, 3.5 μM; a DAD detector with excitation at 354 nm and emission at 450 nm with gradient elution of 10 mM ammonium acetate in water and methanol at flow rate of 0.8 mL·min^{-1} and the injection volume of 30 μL. Extraction was carried out by adding 300 μL of ice-cold methanol to 100 μL of plasma samples, the supernatant was evaporated at 40°C using Turbo Vap LV (Caliper Lifesciences, Mountain View, CA, USA); after evaporation, the samples were reconstituted by adding 100 μL of 10 mM ammonium acetate, pH adjusted to 5.75 with acetic acid and further injected into the HPLC. Data was acquired using Chemstation 3D software (Agilent).

HLM, human intestinal microsomes (HIM), CYP isoenzymes and UGT isoenzymes

Phase I metabolism of 13-cRA was measured using HLM, HIM, and different cDNA-expressed CYP isoforms: CYP3A5, CYP3A4, CYP2C19, CYP2C8, CYP2C9*3, CYP2C9*1, CYP2C9 and CYP2B6. 13-cRA or 4-oxo-13-cRA were incubated with mixtures containing enzyme fractions (0.5 mg·mL^{-1} total protein), the NADPH generating system consisting of solutions A and B (BD Gentest) and 0.1 M potassium phosphate buffer (pH 7.4). To block specific isoenzyme activity we used inhibitors of CYP3A4 (ketoconazole), CYP2C9 (fluconazole), and CYP2C8 inhibitor (gemfibrozil). The inhibitors were added to the incubation mixture before adding the substrates. For glucuronidation of 13-cRA and 4-oxo-13-cRA, various

cDNA expressing UGT isoforms were used (UGT1A1, UGT1A3, UGT1A7, UGT1A8 and UGT1A9). The incubation mixture consisted of 13-cRA or 4-oxo-13-cRA, enzyme fractions (0.5 mg·mL^{-1} total protein), alamethicin (a pore-forming peptide that enhances conjugation rates, 25 μg·mL^{-1}), $MgCl_2$ (8 mM), UDPGA (provides glucuronosyl group to substrates for glucuronidation, 2 mM), methanol (vehicle for substrates, 0.25 %) and Tris-HCL buffer (50 mM, pH 7.5). The reaction mix was incubated for 60 min at 37°C in a shaking water bath, and the reaction was stopped by adding ice-cold methanol with internal standard. The samples were analysed using an HPLC system as described above. Substrate concentrations and velocity data for metabolites were fitted by the hyperbolic Michaelis–Menten model (Rubin and Tozer, 1986).

Enzyme induction in human hepatocytes

Freshly plated human hepatocytes (GIBCO, Invitrogen catalog no. HMFY06) were incubated with 13-cRA to assess enzyme induction by the drug. Cells were maintained in phenol red free Williams E medium at 37°C in humidified incubators with 5% CO2. Shipping medium from the hepatocytes was carefully aspirated and replaced with supplementing medium (Williams E medium + penicillin/streptomycin, ITS, Glutamax, HEPES) and the cells were incubated overnight. Medium was replaced daily, and the cells were treated with either 13-cRA or vehicle for 72 h. Then, mRNA was extracted from the cells using RNeasy Mini Kit (Qiagen).

Statistical analysis

Student's *t*-test was used to determine statistically significant differences on MS Excel. *P*-values were two sided and tests were considered significant at $P < 0.05$. All the experiments were performed in triplicate and were consistently repeatable; for simplicity, one representative experiment for each condition is shown.

Drugs, chemicals and other reagents

Isotretinoin (13-cRA) was obtained from Sigma-Aldrich (St Louis, MO, USA). 4-oxo-13-cRA was obtained from Toronto Research Chemical Inc. Stock solutions of 5 mM were made in absolute ethanol for both compounds and kept in dark at –20°C. Antibodies for MYCN and RARβ (detecting RARβ1 and 2) were purchased from Santa Cruz Biotechnology, Inc. (Dallas, TX, USA). Propidium iodide (PI) was purchased from Molecular Probes, fluorescein diacetate from Eastman Kodak Company, eosin Y from Sigma Chemical Co., and Alexa Fluor 488® phalloidin from Life Technologies. Ketoconazole, gemfibrozil and fluconazole were from Sigma-Aldrich. CYP reaction mix, NADPH regenerating system, Solution A (NADP+ and Glc-6-PO4) and Solution B (G6PDH) and UGT reaction mix, Solution A [25 mM uridine diphosphoglucuronic acid UDPGA)] and Solution B (5X-UGT assay buffer with alamethicin) were purchased from BD Gentest (current vendor: Corning Life Sciences, Union City, CA, USA). Pooled human liver and intestinal microsomes and the recombinant human CYP3A5, CYP3A4, CYP2C19, CYP2C8, CYP2C9*3, CYP2C9*1, CYP2C9, CYP2B6, UGT1A1, UGT1A3, UGT1A7, UGT1A8, UGT1A9, UGT2B4, UGT2B7 and UGT2B isoenzymes were also obtained from BD Gentest.

Results

Identification of 13-cRA metabolites in plasma of patients treated with 13-cRA

Using LC/MS/MS, we identified 13-cRA metabolites in plasma samples from seven patients treated with 160 mg·m^{-2}·day^{-1} of 13-cRA. Figure 1 shows the spectra of the metabolites identified in patient plasma samples. We identified six metabolites (peak area ratio >0.02 relative to the parent drug in humans). Quantitative Optimization on 13-cRA was performed to determine the major fragments. An IDA-based theoretically created Multi-MRM survey scan with two EPI (MS2) as well as neutral loss experiments were set up for the detection of metabolites. The product ion spectrum of the ions at *m/z* 301 and *m/z* 315 confirmed the parent drug 13-cRA and the predominant metabolite 4-oxo-13-cRA. The declustering potential of 30 was used to detect phase II metabolites of the drug. The metabolites showed [M + H] + ions at *m/z* 491 and *m/z* 477 and their fragment spectra corresponding to the addition of glucuronide to 4-oxo-13-cRA and 13-cRA. Methylated 13-cRA ion of [M + H] + ion at *m/z* 315 and mono-hydroxy-13-cRA (13-cRA-OH) ion of [M + H] + ion at 317 were detected. Although the intensity was low, we were able to identify GSH conjugated 4-oxo-13-cRA in some plasma samples by the neutral loss of 129 (confirming a GSH adduct) in nine of 27 patients. Screen capture images of the mass spectra of the metabolites are shown in Supporting Information Fig. S1.

Identification of isoenzymes responsible for 13-cRA metabolism

Detection of 4-oxo-13-cRA in patient samples treated with 13-cRA prompted us to identify the important CYP isoforms responsible for 13-cRA oxidation. As the CYP enzymes are present in liver and intestine in humans, we first compared the 4-oxo-13-cRA formation using pooled HLM and pooled HIM (Figure 2A left column). Based on Michaelis–Menten enzyme kinetic analysis, the V_{max} values were more than fivefold greater for HLM (11.81) compared with that for HIM (2.17; Table 1), and also, the K_m values were 10-fold greater for HIM compared with HLM (1133.1 vs. 12.3 μM).

To identify the isoenzyme(s) for the conversion of 13-cRA to 4-oxo-13-cRA, we used seven recombinant CYP isoforms (CYPs 3A4, 3A5, 2C8, 2C19, 2C9*1, 2C9*3 and 2B6; Figure 2A). Even though the V_{max} was the highest for CYP2B6 (>150), CYP3A4 (16.6) was the major isoenzyme for 13-cRA oxidation as V_{max} for CYP2B6 did not reach plateau (not achievable *in vivo*). In addition, the levels of CYP2C19 mRNA are significantly lower in humans than that of CYP3A4 (Nishimura *et al.*, 2003). K_m values were the lowest for CYP3A4 compared with all the different CYP isoforms analysed. 4-oxo-13-cRA formation by CYP2C8 appears to be similar to CYP3A4, but the K_m for CYP2C8 (64.2) was higher than that for CYP3A4 (41.0). To confirm the role of these enzymes in the formation of 4-oxo-13-cRA from 13-cRA, we incubated 13-cRA in HLM with the NADPH generating system along with ketoconazole (CYP3A4 inhibitor), fluconazole (CYP2C9 inhibitor), or gemfibrozil (CYP2C8 inhibitor). The formation of 4-oxo-13-cRA was significantly reduced by all three inhibitors with the highest inhibitory

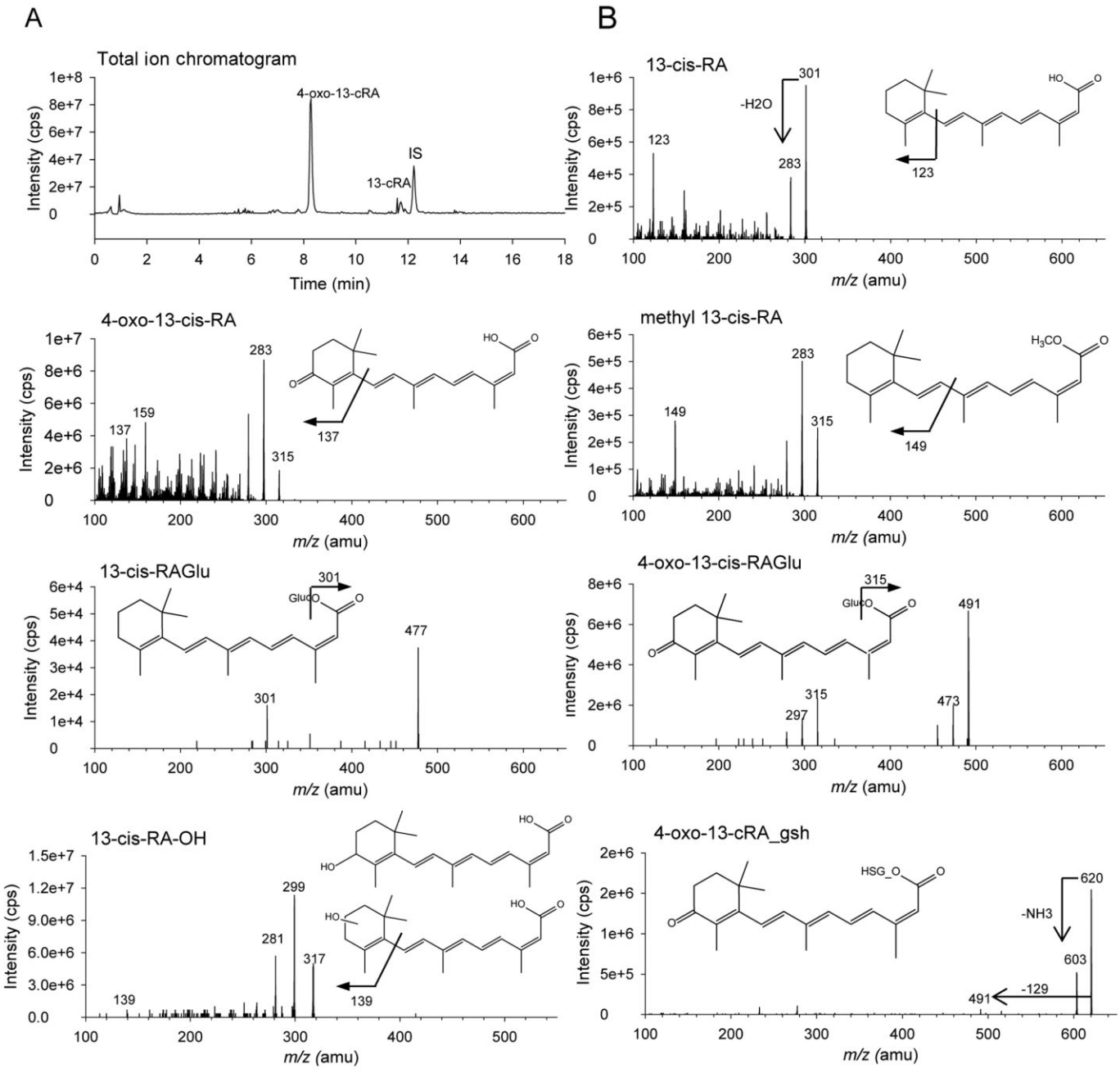

Figure 1

Identification of 13-cRA metabolites in plasma of 13-cRA-treated patient. (A) HPLC chromatograms showing peaks for 13-cRA metabolites. The metabolites that were identified using tandem MS were absent in the HPLC chromatogram except for 4-oxo-13-cRA. (B) Structural identification of metabolites via MS/MS.

effect (>80%) seen with ketoconazole (Figure 2B). These data suggest that CYP3A4 plays a major role in the formation of 4-oxo-13-cRA.

To determine whether 13-cRA induced the metabolizing enzymes, we incubated fresh human hepatocytes with 13-cRA as described in the Methods. At the end of 72 h, we observed that the mRNA levels of the major CYP isoenzymes (CYP2C19, CYP3A4 and CYP3A5) were two- to threefold increased by 13-cRA treatment while CYP2C9, CYP2B6 and CYP2C8 expression were 0.3- to 3-fold decreased relative to vehicle control ($P < 0.05$; Figure 2C).

We then performed mouse experiments to determine whether enzyme induction by 13-cRA was observed *in vivo*. BALB/c mice were treated with 13-cRA twice daily up to 5 days as described in the Methods. The animals were killed and the liver and plasma samples were collected on days 1, 3

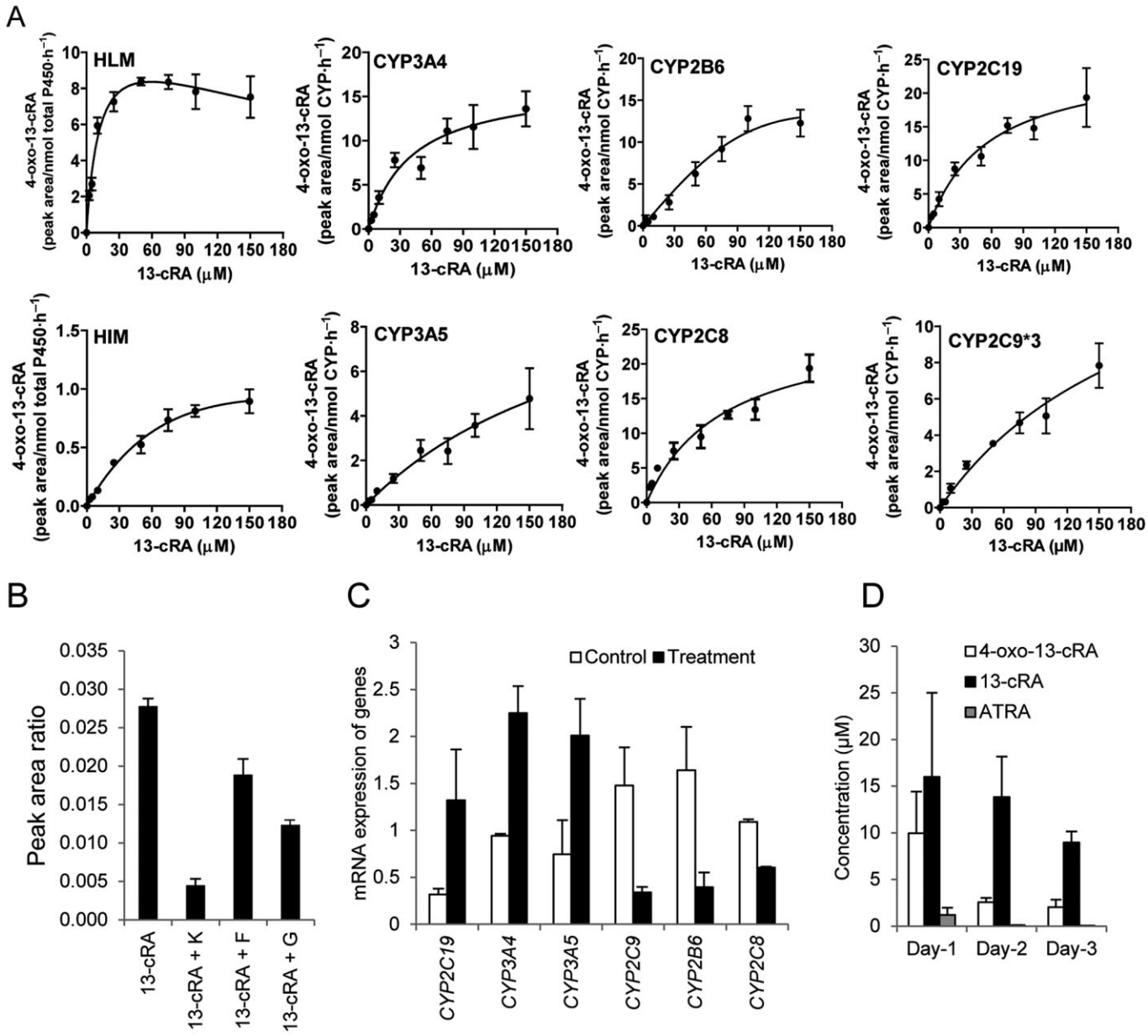

Figure 2

In vitro metabolism of 13-cRA in pooled human liver (HLM), intestinal (HIM) microsomes and recombinant CYP P450 isoforms. (A) Rate of 4-oxo-13-cRA formation by HLM and HIM and various CYP isoforms CYP3A4, CYP3A5, CYP2C9*1, CYP2C9*3, CYP2C8 and CYP2C9. Substrate concentration range was from 0–100 μM and incubations were performed in triplicate. Amounts of metabolites measured by HPLC were normalized to the amount of HLM, HIM and CYP isoenzyme protein levels respectively. Data are shown as ± SEM. Time for incubation and protein concentration and linearity of assay were optimized in preliminary studies. (B) Pharmacological inhibition of enzyme reaction. Pooled HLM were incubated with 5 μM 13-cRA with or without 50 μM ketoconazole (K), 50 μM fluconazole (F), or 100 μM gemfibrozil (G) for 60 min. The reaction was stopped by adding ice-cold methanol with internal standard. The samples were analysed by HPLC to determine the peak ratio of 4-oxo-13-cRA to 4-HPR (internal standard). (C) mRNA levels of CYP P450 isoenzymes in the human hepatocytes treated with or without 5 μM 13-cRA. After 72 h of treatment, hepatocytes were detached by scrapping and mRNA levels of CYP3A4, CYP3A5, CYP2C19, CYP2C9, CYP2B6 and CYP2C8 were analysed by real-time RT-PCR. (D) Plasma levels of 13-cRA and its metabolites (4-oxo-13-cRA and ATRA) in BALB/c mice treated with 13-cRA at 53 $mg \cdot kg^{-1} \cdot day^{-1}$ (human equivalent dose of 160 $mg \cdot m^{-2} \cdot day^{-1}$). Blood samples were collected on days 1, 3 and 5 from the mice by cardiopuncture ($n = 4$).

and 5 (Figure 2D). In mice, the plasma concentrations of 4-oxo-13-cRA were lower than those of 13-cRA for the duration of the study. In addition, the mRNA and protein levels of the enzymes did not significantly change over 5 days (data not shown), indicating that the metabolism of 13-cRA in mice is different from that of humans.

The identification of 4-oxo-13-cRA glucuronide in patient plasma samples prompted us to characterize glucuronidation

Table 1

Apparent V_{max} and K_m for 4-oxidation of 13-cRA to its metabolite 4-oxo-13-cRA and the glucuronidation of 13-cRA to 13-cRA glucuronide

	V_{max}	K_m (μM)
4-oxo-13-cRA formation by		
CYP3A4	16.57	40.97
CYP3A5	13.20	>150
CYP2C19	25.19	55.77
CYP2C8	23.89	64.24
CYP2B6	>150	>150
CYP2C9*3	17.8	>150
HLM	11.81	12.30
HIM	2.17	133.1
13-cis-RA glucuronide formation by		
UGT1A1	0.21	66.5
UGT1A3	14.9	35.1
UGT1A7	0.01	<20
UGT1A8	0.86	26.0
UGT1A9	0.03	19.4

The unit for V_{max} is (normalized peak area)/nmol CYP·h^{-1} for CYP enzymes, HLM and HIM. For glucuronidation reaction, V_{max} is expressed as (normalized peak area)/nmol UGT·h^{-1}.

of 13-cRA by UGT isoenzymes. To determine the differences in glucuronidation rate between 4-oxo-13-cRA and 13-cRA, and to identify UGT isoenzymes responsible for glucuronidation, various recombinant UGT isoforms UGTs 1A1, 1A3, 1A7, 1A8, 1A9, 2B4, 2B7, 2B15, 2B17, HLM and HIM were incubated with 4-oxo-13-cRA and 13-cRA as described in and the Methods. In HIM and HLM, 13-cRA glucuronidation rates appear to be higher than 4-oxo-glucuronidation, although substrate inhibition was suspected at higher concentrations of 13-cRA tested, and thus V_{max} and K_m were not determined (Supporting Information Fig. S2). Unlike the glucuronidation of 13-cRA that plateaus at higher substrate concentrations, the glucuronidation of 4-oxo-13-cRA showed much higher rates in the presence of UGT1A isoenzymes although V_{max} and K_m were not determined due to the fact that saturation did not occur at higher 4-oxo-13-cRA concentrations up to 200 μM (Supporting Information Fig. S2; V_{max} and K_m values for 13-cRA glucuronidation are included in Table 1). Glucuronidation products by all UGT2B isoenzymes were not seen up to 150 μM (the highest concentration tested) for 13-cRA and up to 25 μM for 4-oxo-13-cRA (Supporting Information Fig. S2). In NB patients, the mean concentration of 13-cRA on day 14 of treatment was 2.83 μM which was significantly lower that the levels of 4-oxo-130cRA. In addition, our data showed that 4-oxo-13-cRA glucuronide is more frequently detected in patient plasma than 13-cRA glucuronide, suggesting that oxidation to 4-oxo-13-cRA and further glucuronidation of 4-oxo-13-cRA is the major metabolic pathway of 13-cRA (Figure 3).

Inhibitory effects of 4-oxo-13-cRA and 13-cRA on tumour cell growth and proliferation

To determine if 4-oxo-13-cRA is an active metabolite of 13-cRA, we assessed the anti-proliferation activity of 4-oxo-13-cRA relative to 13-cRA. Six cell lines (three with *MYCN* gene amplification, all established at progressive disease after chemotherapy but from patients who were never treated with 13-cRA) were treated with various concentrations of 4-oxo-13-cRA and 13-cRA for 10 days (Figure 4A). In three cell lines (SMS-KANR, CHLA-20 and SMS-LHN), both 4-oxo-13-cRA and 13-cRA inhibited more than 90% of the growth at the highest concentration tested. The dose–response curves of 13-cRA and those of 4-oxo-13-cRA were not significantly different in all six cell lines ($P > 0.2$ in all six cell lines). The effect of 13-cRA and 4-oxo-13-cRA on cell cycle progression was assessed using flow cytometry (Figure 4B). A significant decrease was observed in the percentage of cells in S-phase when treated with 13-cRA or 4-oxo-13cRA relative to control (22.57 ± 0.91% for control, 5.34 ± 1.47% for 13-cRA and 6.95 ± 0.99% for 4-oxo-13-cRA, $P < 0.0001$, Figure 4C). Thus, there is no significant difference in the inhibitory effects of 13-cRA and 4-oxo-13-cRA on cell proliferation of NB cell lines.

Effect of 4-oxo-13-cRA and 13-cRA on MYCN and RARβ

Amplification of *MYCN* is associated with poor prognosis in NB patients (Caren *et al.*, 2010), and the MYCN protein enhances various tumourigenic properties such as the increase in cell proliferation and insulin-like growth factor type I receptor expression (IGF1R; Fotsis *et al.*, 1999; Pelengaris *et al.*, 2002; Pession and Tonelli, 2005). Because it is known that 13-cRA down-regulates MYCN protein and mRNA expression in NB cells (Reynolds *et al.*, 1991; Hadjidaniel and Reynolds, 2010), we examined the effect of 4-oxo-13-cRA on MYCN down-regulation in a panel of *MYCN*-amplified and *MYCN* non-amplified NB cell lines. Real-time RT-PCR data (Figure 5A) showed a significant decrease ($P < 0.05$) in *MYCN* mRNA levels in cells treated with either 4-oxo-13-cRA or 13-cRA compared with vehicle control, and the *MYCN* mRNA levels were not significantly different between 13-cRA and 4-oxo-13-cRA treatment in *MYCN*-amplified cells (Figure 5A left). In non-*MYCN*-amplified cells, the *MYCN* mRNA were constitutively lower than observed in *MYCN*-amplified cell lines, and thus cRA treatment did not result in a significant decrease in *MYCN* mRNA relative to control with the exception of SMS-LHN (Figure 5A right). A decrease in MYCN protein levels was also apparent in all four *MYCN*-amplified cell lines, including SMS-KANR after cRA treatment, and the extent of the decrease relative to control appears to be the same for both 13-cRA and 4-oxo-13-cRA treatment (Figure 5B).

Retinoic acids mediate their action through two classes of nuclear receptors, retinoic acid receptors (RARs) and retinoid X receptor (RXRs) in NB cells (Reynolds, 2000), which are encoded by three genes α, β and γ (Alvarez *et al.*, 2011). High RARβ expression has been associated with good clinical outcome in NB, and studies have shown that increased expression of the gene by transfection enhances the responsiveness in some NB cell lines to retinoic acids (Cheung *et al.*,

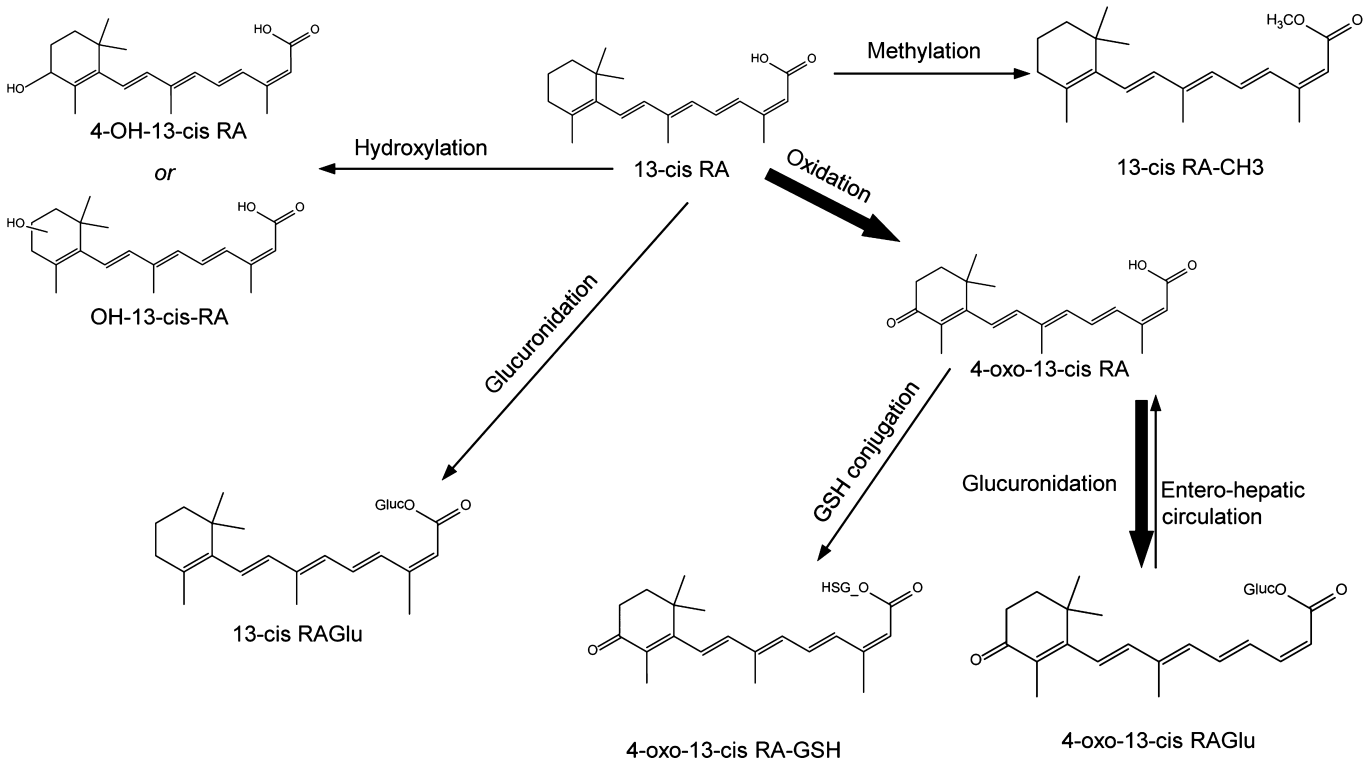

Figure 3

Proposed pathway for 13-cRA metabolism. Major enzymes involved in the interconversion of one metabolite into another, that is, the conversion of 13-cRA to 4-oxo-13-cRA, Dark arrows represent the metabolites found in high concentrations in patient plasma sample compared with other metabolites.

1998). Previous studies showed that ATRA induced RARβ at both protein and mRNA levels (Clagett-Dame *et al.*, 1993; Marshall *et al.*, 1994; Wuarin *et al.*, 1994). Therefore, we compared RARβ induction by 4-oxo-13-cRA to induction by 13-cRA. Real-time RT-PCR showed that both 13-cRA and 4-oxo-13-cRA treatment lead to a significant ($P < 0.05$) induction of *RARB* mRNA levels compared with vehicle control cells on day 10 in four *MYCN* gene-amplified and three *MYCN* non-amplified NB cell lines, and no differences were seen between 13-cRA and 4-oxo-13-cRA in inducing *RARB* ($P = 0.632$; Figure 5C). *RARB* induction was translated into an increase in RARβ protein levels (Figure 5D). Our data showed that the cell lines established from patients with progressive disease after cytotoxic chemotherapy (SMS-LHN, SK-N-BE(2), SMS-KCNR) were responsive to the retinoids, consistent with previous data showing that prior exposure to cytotoxic chemotherapy does not confer resistance to 13-cRA (Reynolds *et al.*, 1991; 1994). This was also observed clinically in NB patients (Villablanca *et al.*, 1995).

4-oxo-13-cRA and 13-cRA promote neurite outgrowth and cell differentiation

13-cRA is a powerful inducer of neurite outgrowth and cell differentiation (Reynolds *et al.*, 2003). Subsequently, we determined whether 4-oxo-13-cRA was able to induce morphological changes (neurite outgrowth) and biochemical differentiation and compared it with the 13-cRA treatment. Upon treatment with 13-cRA and 4-oxo-13-cRA, neurite outgrowth assessed by staining phalloidin was apparent in both SMS-KCNR and SMS-LHN cells (Figure 6A) compared with control. Neurite lengths were significantly longer in cells treated with either 13-cRA or 4-oxo-13-cRA in SMS-KCNR and SMS-LHN cells compared with vehicle control-treated cells ($P < 0.001$; Figure 6B), and no significant differences in the induced neurite lengths was observed between 13-cRA and 4-oxo-13-cRA. To examine biochemical differentiation in cells, the changes in various mature neuronal markers (Map2C and NeuN) were determined by immunoblotting after 10 days of treatment with either 13-cRA or 4-oxo-13-cRA; expression of the neuronal markers was increased in the two NB cell lines by both 13-cRA and 4-oxo-13-cRA (Figure 6C).

Discussion

Based on our data from HLM experiments with pharmacological inhibitors and human fresh hepatocytes, CYP3A4 contributes the most to the oxidation of 13-cRA to 4-oxo-13-cRA, the most abundant metabolite. In addition, CYP3A4 and CYP3A5 expression was induced by 13-cRA treatment in human hepatocytes while other enzymes were not, suggesting that upregulation of the enzyme contributes to the high steady-state concentrations of 4-oxo-13-cRA on day 14 in patients treated with 13-cRA. Although the kinetic profile could not be determined for 4-oxo-13-cRA glucuronidation due to its ability to increase the formation of the glucuronide product at

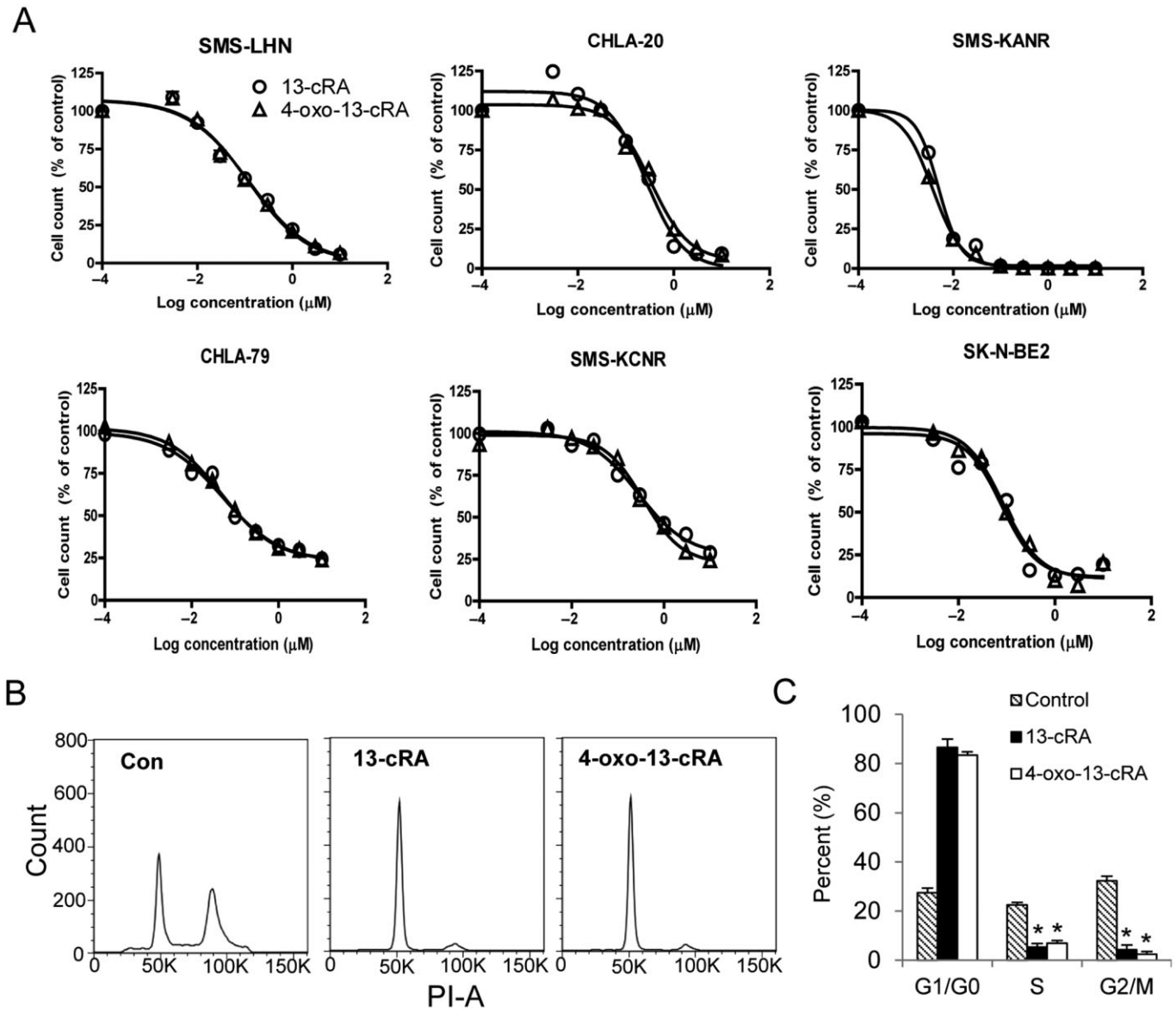

Figure 4

Dose-response curves comparing growth inhibition induced by 13-cRA and 4-oxo-13-cRA treated with a range of concentrations from 1 nM to 10 μM. (A) Cells were plated in three different 96-well plates and treated with both compounds for 10 days and relative fluorescence was assessed by DIMSCAN. Each condition had six replicates and the differences in the inhibitory effects on proliferation between 13-cRA and 4-oxo-13-cRA were evaluated using Student's *t*-test. CHLA-266, an Ewing's family of sarcoma cell line, was used as negative control. Less than 25% of growth inhibition relative to control was observed in CHLA-266 at the highest concentrations (10 μM) of 13-cRA or 4-oxo-13-cRA (data not shown). (B) Cell cycle analysis of SMS-KCNR cells by flow cytometry, to compare the decrease in cell proliferation after a 10 day treatment with 13-cRA and 4-oxo-13-cRA. (C) Flow cytometry data analysed using Flow Jo software. Both treatments showed a similar and significant (*$P < 0.0001$) decrease in the cells in S-phase (proliferative phase) of cell cycle compared with the untreated control cells.

higher concentrations, we observed that much higher peaks of 4-oxo-13-cRA glucuronide were formed across a range of concentrations. Conversion of 13-cRA or ATRA to 4-oxo-13-cRA and 4-oxo-ATRA has been reported. However, there is no evidence that 4-oxo-metabolites convert back to the parent compound. Our HPLC assay data using cultured cell lines showed that 4-oxo-13-cRA does not convert to 13-cRA in cell culture medium or in NB cells (data not shown). Thus, our data demonstrated that metabolism of 13-cRA to 4-oxo-13-cRA and further glucuronidation of the metabolite is the major metabolism pathway of the drug in humans.

Because of the levels of 4-oxo-13-cRA observed in patient plasma and it being the key metabolic product of 13-cRA, we assessed whether this metabolite [previously considered to be inactive (Veal *et al.*, 2007)] has anti-NB activity. We demonstrated conclusively that 4-oxo-13-cRA is as active as 13-cRA in inducing differentiation of various NB cell lines regardless of their *MYCN* amplification status, and that 4-oxo-13-cRA

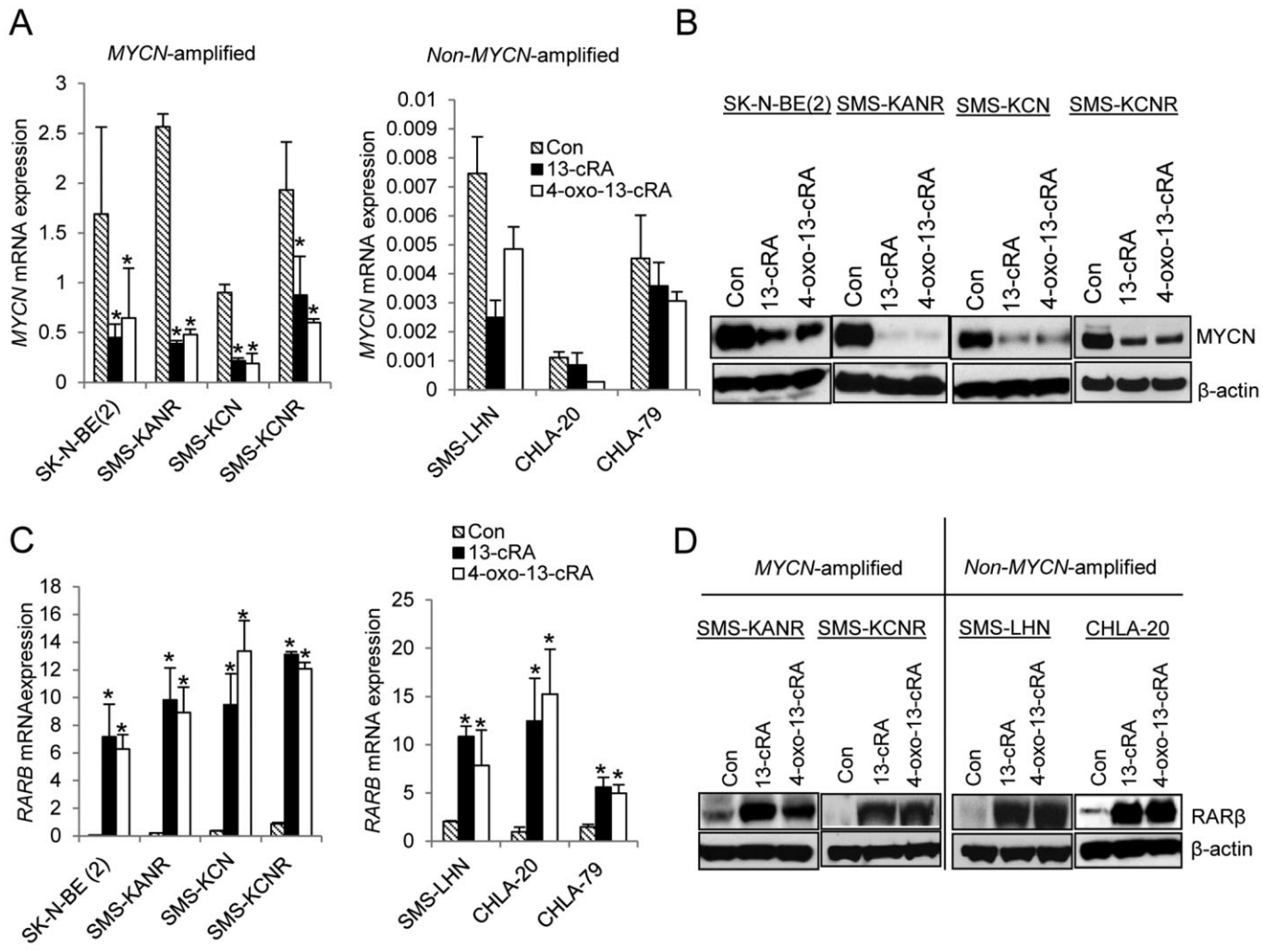

Figure 5

Effect of 4-oxo-13-cRA on *MYCN* and *RARB* in comparison with 13-cRA. Cells were treated with 13-cRA or 4-oxo-13-cRA for 10 days and protein and mRNA was extracted on the 10th day. (A, B) Real-time RT-PCR analysis of *MYCN* mRNA and protein expression in *MYCN* amplified cells (SK-N-BE2, SMS-KANR, SMS-KCN and SMS-KCNR, A left) and in *MYCN* non-amplified cells (SMS-LHN, CHLA-20 and CHLA-79, A right). Immunoblotting analysis showed the decrease in the MYCN levels after the treatments with retinoids as compared with the controls in *MYCN* gene-amplified cells (SK-N-BE2, SMS-KANR, SMS-KCN and SMS-KCNR, B). In *MYCN* non-amplified cells, MYCN protein was minimally expressed and thus the data are not included. (C, D) Real-time RT-PCR analyses of *RARB* mRNA expression in *MYCN* amplified cell lines and *MYCN* non-amplified cell lines. *MYCN*-amplified cells (SK-N-BE2, SMS-KANR, SMS-KCNR, and SMS-KCN) and *MYCN* non-amplified cells (SMS-LHN, CHLA-20 and CHLA-15), were treated with 13-cRA or 4-oxo-13-cRA for 10 days, and mRNA expression of *RARB* (by real-time RT-CPR, C) and RARβ levels (immunoblotting, D) were measured. *$P < 0.05$.

inhibits cell proliferation, down-regulates the expression of *MYCN*, and induces the expression of *RARB*. *MYCN* genomic amplification and consequent overexpression of the protein is one of the adverse prognostic factors for NB. Many studies suggest that *MYCN* down-regulation is critical in the differentiation process, and that the ability of retinoic acids to decrease the expression of *MYCN* is a critical aspect of their anti-NB activity (Thiele *et al.*, 1985; Peverali *et al.*, 1996; Burkhart *et al.*, 2003). A CT-box was identified as the only regulatory motif fully contained within the RA responsive region in NB cell lines (Lutz and Schwab, 1997). Along with E2F, the Sp1 and Sp3 transcription factors are reported to be necessary for *MYCN* down-regulation (Kramps *et al.*, 2004). However, Sp1/Sp3 does not appear to mediate *MYCN* down-regulation in response to RA (Kanemaru *et al.*, 2008). Thus, the mechanism of *MYCN* down-regulation in response to RA treatment remains to be delineated.

High-dose intermittent therapy with 13-cRA achieved clinical responses and used after myeloablative therapy provides a significant improvement in event-free survival of NB patients (Matthay *et al.*, 1999). However, minimal clinical activity and no benefit in survival after myeloablative therapy was observed with continuous low-dose therapy (Finklestein *et al.*, 1992), indicating that the therapeutic activity of 13-cRA is dependent on achieving tumour-effective plasma levels of the drug. There is a large interpatient variability in the plasma concentrations achieved after exposure to 13-cRA in NB patients, with plasma concentrations of 13-cRA measured at

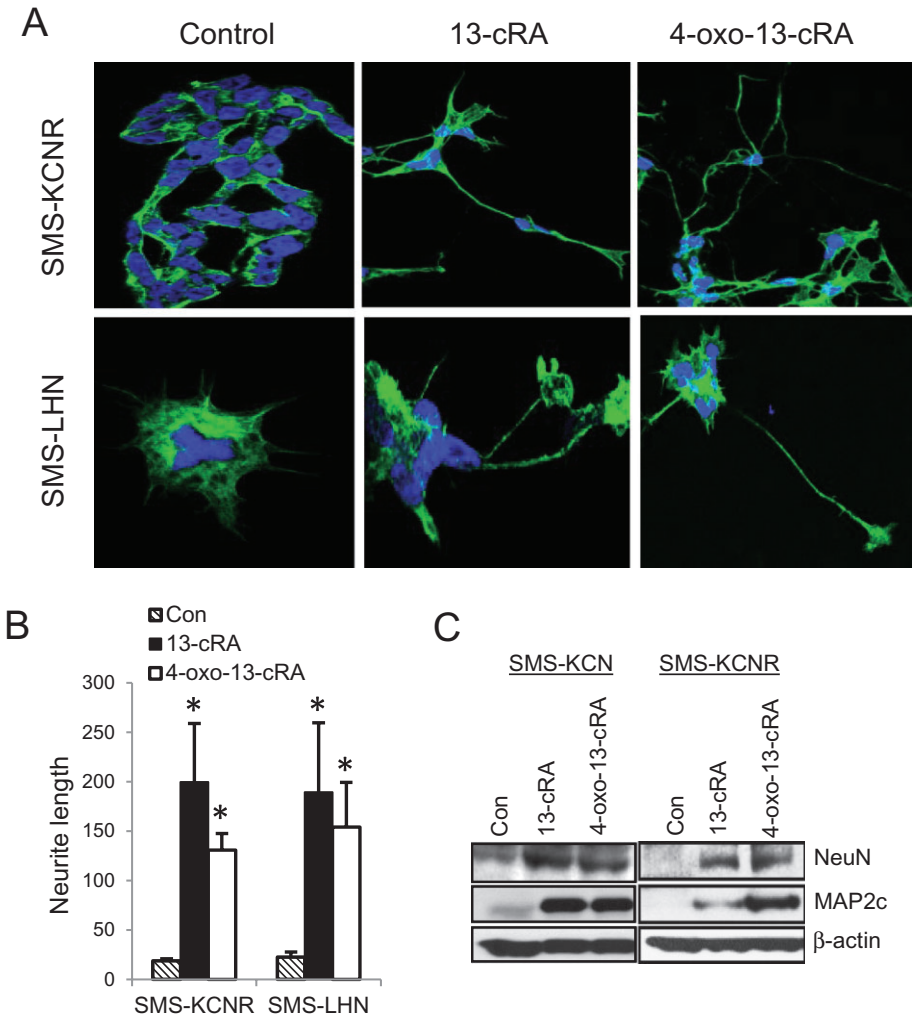

Figure 6

Neurite outgrowth induced by 4-oxo-13-cRA and 13-cRA in NB cell lines. SMS-KCNR, a *MYCN* gene-amplified cell line and SMS-LHN, a *MYCN* non-amplified cell line were treated with 13-cRA and 4-oxo-13-cRA for 10 days, and neurite outgrowth was assessed by confocal microscopy and the expression of cell differentiation markers was evaluated by immunoblotting. (A) SMS-KCNR and SMS-LHN, control and treated cells were stained with Alexa Flour 488 phalloidin and analysed by confocal microscopy. Nucleus was stained with DAPI (blue). (B) To quantify the neurite outgrowth, confocal *z*-stack projections (60X) were used for analysis, and the fluorescence intensity was assessed by Metamorph analysis software in Alexa Fluor 488 stained cells (*$P < 0.001$). (C) Differentiation of SMS-KCN and SMS-KCNR cells treated with both 13-cRA (5 μM) and 4-oxo-13-cRA (5 μM) was compared by the changes in mature neuronal markers (NeuN and Map2c) by immunoblotting.

steady state varying >10-fold among patients who received the same dose of 13-cRA (Veal *et al.*, 2007). It is unclear whether the variability is due to difficulties in administering the only available formulation of 13-cRA (capsules) to the young children being treated for NB or to other issues, such as differences in metabolism.

Therapeutic monitoring of the plasma concentrations to adjust the dose of the drug has been proposed (Veal *et al.*, 2007; 2013). However, the proposed dose adjustments are based on the assumption that the major metabolite of 13-cRA, 4-oxo-13-cRA, is inactive. Indeed, data used to support dose adjustments of 13-cRA for NB patients show that 4-oxo-13-cRA concentrations were greater than twofold higher than those of 13-cRA in plasma with 160 $mg \cdot m^{-2} \cdot day^{-1}$ of 13-cRA (Veal *et al.*, 2007; 2013). Our current study shows that 13-cRA and 4-oxo-13-cRA are equally active against NB cells. The 13-cRA dose modifications proposed for NB patients based on age (Veal *et al.*, 2013) were developed by examining the plasma levels of only 13-cRA, rather than concentrations of both 13-cRA and 4-oxo-13-cRA. Our data clearly indicate that identifying patients that may benefit from an increase in 13-cRA dose require consideration of the parent drug and the 4-oxo-13-cRA active metabolite. Basing dose adjustments on the parent drug alone may result in an inappropriate higher dose for some patients (which could lead to increased systemic toxicities) than is necessary for achieving anti-NB activity. As the dosing of 13-cRA established in the CCG phase I study (Villablanca *et al.*, 1995) has demonstrated a significant increase in event-free survival (Matthay *et al.*, 1999), it is highly unlikely that the majority of patients were achieving the low levels of active drug suggested in the recent PK studies (Veal *et al.*, 2013).

An aspect of 13-cRA PK requiring further exploration is the observation that patients who received 13-cRA via the same method (e.g. swallowed intact capsules vs. extracted drug in capsules) achieved up to 10-fold differences in plasma concentrations of the drug and the metabolite, indicating that in some patients, the differences in achieved 13-cRA plasma levels may be due to factors other than reduced drug amount extracted from the capsules prior to dosing. Our data with liver microsomes points towards the potential for enzymatic polymorphisms being responsible for different PK profiles in some patients. Knockout animal models of several metabolizing enzymes that we identified in the current manuscript could potentially confirm these results. However, as shown in our data, 4-oxo-13-cRA levels in mice were not as high as in humans, suggesting that mice metabolize 13-cRA differently from humans. Therefore, the optimal approach to this issue will be robust studies of 13-cRA pharmacokinetics in relation to pharmacogenomics and treatment outcome in a large number of patients. A large pharmacokinetic and pharmacogenomics study of 13-cRA is currently underway in the COG.

13-cRA has been studied as a potential chemopreventive agent in non-small cell lung cancer due to its effect on RARβ and has demonstrated clinical utility in preventing secondary cancers in patients with head and neck cancer (Lippman *et al.*, 1988; Khuri *et al.*, 2006). Although large phase III studies were unable to demonstrate any benefit of 13-cRA in primary, secondary or tertiary prevention of lung cancer (Lippman *et al.*, 2001), studies have identified that former smokers but not current smokers may benefit from the drug which might be related to its ability to upregulate *RAR*β, the gene that is epigenetically silenced in the early stage of lung cancer (Kim *et al.*, 2004). Unfortunately, pharmacokinetic properties of 13-cRA were not assessed in the prevention studies, and the initial dose given to patients was 0.5 $mg \cdot kg^{-1} \cdot day^{-1}$, which is approximately 1/10 of the dose being used in NB patients. This makes the comparison of the drug activity between NB studies and the prevention studies in adults difficult to undertake. Perhaps more relevant to this study are the chemoprevention studies of secondary head and neck cancers that have demonstrated a significant effect of 13cRA as a chemopreventive in that setting (Lippman *et al.*, 1988; Khuri *et al.*, 2006). While it is tempting to speculate that improved chemoprevention could be achieved with more optimal dosing strategies and thus higher 13-cRA exposures in those adult chemopreventive trials, the tolerability and feasibility of such dosing strategies in the adult population is unknown. Thus, we feel our data best address the use of 13-cRA in paediatric NB, but our documentation that 4-oxo-13-cRA is an active metabolite of 13-cRA in NB indicates that it may also be active in the chemoprevention setting. In addition, a biological aspect of RAR needs to be considered when assessing the effect of 13-cRA in tumours. RARs and RXRs can heterodimerize with other types of receptors, including oestrogen receptor-α (Hua *et al.*, 2009) PPAR (Schug *et al.*, 2007), and other receptors to regulate their partner receptor's pathways which may result in the up-regulation of prosurvival genes. This is contrary to the known differentiation function of RARs and RXRs in response to retinoic acid and should be studied further to determine the role of RA in cell death pathways.

In conclusion, we have defined the metabolic pathways for 13-cRA and we have shown that 4-oxo-13-cRA, the most abundant metabolite with much higher levels than 13-cRA in patients, is as effective as 13-cRA in producing prolonged growth arrest, differentiation and MYCN down-regulation. Our data will inform the interpretation of any studies seeking an association between the pharmacokinetics of 13-cRA and clinical outcome. Our data also indicate the need to take into account plasma levels achieved for both 13-cRA and 4-oxo-13-cRA for determining any changes in the dosing schedule relative to dosing that was established in a phase I study (ref) and validated as effective in a randomized phase III study.

Acknowledgements

This work was supported by R01CA CA168699-01 from the National Cancer Institute, RP130547 from Cancer Prevention and Research Institute of Texas and 3U10 CA098543-08S3 from National Institute of Child Health and Human Development. We thank Hardeep Singh for his technical support in measuring some of the 13-cRA, ATRA and 4-oxo-13-cRA concentrations in various laboratory samples.

Author contributions

P. S., H. E. C., A. T. and D. V. conducted experiments; A. L. Y., C. P. R., M. H. K. designed experiments, C. P. R. and M. H. K. wrote the manuscript.

Conflict of interest

No conflict of interest is declared.

References

Abemayor E, Sidell N (1989). Human neuroblastoma cell lines as models for the in vitro study of neoplastic and neuronal cell differentiation. Environ Health Perspect 80: 3–15.

Alexander SPH, Benson HE, Faccenda E, Pawson AJ, Sharman JL, Spedding M *et al.* (2013a). The Concise Guide to PHARMACOLOGY 2013/14: nuclear hormone receptors. Br J Pharmacol 170: 1652–1675.

Alexander SPH, Benson HE, Faccenda E, Pawson AJ, Sharman JL, Spedding M *et al.* (2013b). The Concise Guide to PHARMACOLOGY 2013/14: enzymes. Br J Pharmacol 170: 1797–1867.

Alvarez S, Bourguet W, Gronemeyer H, de Lera AR (2011). Retinoic acid receptor modulators: a perspective on recent advances and promises. Expert Opin Ther Pat 21: 55–63.

Burkhart CA, Cheng AJ, Madafiglio J, Kavallaris M, Mili M, Marshall GM *et al.* (2003). Effects of MYCN antisense oligonucleotide administration on tumorigenesis in a murine model of neuroblastoma. J Natl Cancer Inst 95: 1394–1403.

Caren H, Kryh H, Nethander M, Sjoberg RM, Trager C, Nilsson S *et al.* (2010). High-risk neuroblastoma tumors with 11q-deletion display a poor prognostic, chromosome instability phenotype with later onset. Proc Natl Acad Sci U S A 107: 4323–4328.

Cheung B, Hocker JE, Smith SA, Norris MD, Haber M, Marshall GM (1998). Favorable prognostic significance of high-level retinoic acid receptor beta expression in neuroblastoma mediated by effects on cell cycle regulation. Oncogene 17: 751–759.

Clagett-Dame M, Verhalen TJ, Biedler JL, Repa JJ (1993). Identification and characterization of all-trans-retinoic acid receptor transcripts and receptor protein in human neuroblastoma cells. Arch Biochem Biophys 300: 684–693.

Finklestein JZ, Krailo MD, Lenarsky C, Ladisch S, Blair GK, Reynolds CP *et al.* (1992). 13-cis-retinoic acid (NSC 122758) in the treatment of children with metastatic neuroblastoma unresponsive to conventional chemotherapy: report from the Children's Cancer Study Group. Med Pediatr Oncol 20: 307–311.

Fotsis T, Breit S, Lutz W, Rossler J, Hatzi E, Schwab M *et al.* (1999). Down-regulation of endothelial cell growth inhibitors by enhanced MYCN oncogene expression in human neuroblastoma cells. Eur J Biochem 263: 757–764.

Frgala T, Kalous O, Proffitt RT, Reynolds CP (2007). A fluorescence microplate cytotoxicity assay with a 4-log dynamic range that identifies synergistic drug combinations. Mol Cancer Ther 6: 886–897.

Greenberg BR, Durie BG, Barnett TC, Meyskens FL Jr (1985). Phase I-II study of 13-cis-retinoic acid in myelodysplastic syndrome. Cancer Treat Rep 69: 1369–1374.

Hadjidaniel MD, Reynolds CP (2010). Antagonism of cytotoxic chemotherapy in neuroblastoma cell lines by 13-cis-retinoic acid is mediated by the antiapoptotic Bcl-2 family proteins. Mol Cancer Ther 9: 3164–3174.

Haussler M, Sidell N, Kelly M, Donaldson C, Altman A, Mangelsdorf D (1983). Specific high-affinity binding and biologic action of retinoic acid in human neuroblastoma cell lines. Proc Natl Acad Sci U S A 80: 5525–5529.

Hua S, Kittler R, White KP (2009). Genomic antagonism between retinoic acid and estrogen signaling in breast cancer. Cell 137: 1259–1271.

Iwanaka T, Yamamoto K, Ogawa Y, Arai M, Ito M, Kishimoto H *et al.* (2001). Maturation of mass-screened localized adrenal neuroblastoma. J Pediatr Surg 36: 1633–1636.

Kanemaru KK, Tuthill MC, Takeuchi KK, Sidell N, Wada RK (2008). Retinoic acid induced downregulation of MYCN is not mediated through changes in Sp1/Sp3. Pediatr Blood Cancer 50: 806–811.

Kang MH, Wan Z, Kang Y, Sposto R, Reynolds CP (2008). Mechanism of synergy of *N*-(4-hydroxyphenyl)retinamide and ABT-737 in acute lymphoblastic leukemia cell lines: Mcl-1 inactivation. J Natl Cancer Inst 100: 580–595.

Kang MH, Smith MA, Morton CL, Keshelava N, Houghton PJ, Reynolds CP (2010). National cancer institute pediatric preclinical testing program: model description for in vitro cytotoxicity testing. Pediatr Blood Cancer 56: 239–249.

Keshelava N, Seeger RC, Groshen S, Reynolds CP (1998). Drug resistance patterns of human neuroblastoma cell lines derived from patients at different phases of therapy. Cancer Res 58: 5396–5405.

Khan AA, Villablanca JG, Reynolds CP, Avramis VI (1996). Pharmacokinetic studies of 13-cis-retinoic acid in pediatric patients with neuroblastoma following bone marrow transplantation. Cancer Chemother Pharmacol 39: 34–41.

Khuri FR, Lee JJ, Lippman SM, Kim ES, Cooper JS, Benner SE *et al.* (2006). Randomized phase III trial of low-dose isotretinoin for prevention of second primary tumors in stage I and II head and neck cancer patients. J Natl Cancer Inst 98: 441–450.

Kilkenny C, Browne W, Cuthill IC, Emerson M, Altman DG (2010). Animal research: reporting *in vivo* experiments: the ARRIVE guidelines. Br J Pharmacol 160: 1577–1579.

Kim JS, Lee H, Kim H, Shim YM, Han J, Park J *et al.* (2004). Promoter methylation of retinoic acid receptor beta 2 and the development of second primary lung cancers in non-small-cell lung cancer. J Clin Oncol 22: 3443–3450.

Kramps C, Strieder V, Sapetschnig A, Suske G, Lutz W (2004). E2F and Sp1/Sp3 Synergize but are not sufficient to activate the MYCN gene in neuroblastomas. J Biol Chem 279: 5110–5117.

Kreissman SG, Seeger RC, Matthay KK, London WB, Sposto R, Grupp SA *et al.* (2013). Purged versus non-purged peripheral blood stem-cell transplantation for high-risk neuroblastoma (COG A3973): a randomised phase 3 trial. Lancet Oncol 14: 999–1008.

Li C, Einhorn PA, Reynolds CP (1994). Expression of retinoic acid receptors alpha, beta, and gamma in human neuroblastoma cell lines. Prog Clin Biol Res 385: 221–227.

Lippman SM, Kessler JF, Al-Sarraf M, Alberts DS, Itri LM, Mattox D *et al.* (1988). Treatment of advanced squamous cell carcinoma of the head and neck with isotretinoin: a phase II randomized trial. Invest New Drugs 6: 51–56.

Lippman SM, Lee JJ, Karp DD, Vokes EE, Benner SE, Goodman GE *et al.* (2001). Randomized phase III intergroup trial of isotretinoin to prevent second primary tumors in stage I non-small-cell lung cancer. J Natl Cancer Inst 93: 605–618.

London WB, Castel V, Monclair T, Ambros PF, Pearson ADJ, Cohn SL *et al.* (2011). Clinical and biologic features predictive of survival after relapse of neuroblastoma: a report from the international neuroblastoma risk group Project. J Clin Oncol 29: 3286–3292.

Lutz W, Schwab M (1997). In vivo regulation of single copy and amplified N-myc in human neuroblastoma cells. Oncogene 15: 303–315.

Maris JM, Matthay KK (1999). Molecular biology of neuroblastoma. J Clin Oncol 17: 2264–2279.

Maris JM, Hogarty MD, Bagatell R, Cohn SL (2007). Neuroblastoma. Lancet 369: 2106–2120.

Marshall GM, Cheung B, Stacey KP, Norris MD, Haber M (1994). Regulation of retinoic acid receptor alpha expression in human neuroblastoma cell lines and tumor tissue. Anticancer Res 14: 437–441.

Masters JR, Thomson JA, Daly-Burns B, Reid YA, Dirks WG, Packer P *et al.* (2001). Short tandem repeat profiling provides an international reference standard for human cell lines. PNAS 98: 8012–8017.

Matthay KK, O'Leary MC, Ramsay NK, Villablanca J, Reynolds CP, Atkinson JB *et al.* (1995). Role of myeloablative therapy in improved outcome for high risk neuroblastoma: review of recent Children's Cancer Group results. Eur J Cancer 31A: 572–575.

Matthay KK, Villablanca JG, Seeger RC, Stram DO, Harris RE, Ramsay NK *et al.* (1999). Treatment of high-risk neuroblastoma with intensive chemotherapy, radiotherapy, autologous bone marrow transplantation, and 13-cis-retinoic acid. Children's Cancer Group. N Engl J Med 341: 1165–1173.

Matthay KK, Reynolds CP, Seeger RC, Shimada H, Adkins ES, Haas-Kogan D *et al.* (2009). Long-term results for children with high-risk neuroblastoma treated on a randomized trial of myeloablative therapy followed by 13-cis-retinoic acid: a Children's Oncology Group study. J Clin Oncol 27: 1007–1013.

McGrath JC, Drummond GB, McLachlan EM, Kilkenny C, Wainwright CL (2010). Guidelines for reporting experiments involving animals: the ARRIVE guidelines. Br J Pharmacol 160: 1573–1576.

Nishimura M, Yaguti H, Yoshitsugu H, Naito S, Satoh T (2003). Tissue distribution of mRNA expression of human cytochrome P450 isoforms assessed by high-sensitivity real-time reverse transcription PCR. Yakugaku Zasshi 123: 369–375.

Park JR, Villablanca JG, London WB, Gerbing RB, Haas-Kogan D, Adkins ES *et al*. (2009). Outcome of high-risk stage 3 neuroblastoma with myeloablative therapy and 13-cis-retinoic acid: a report from the Children's Oncology Group. Pediatr Blood Cancer 52: 44–50.

Park JR, Bagatell R, London WB, Maris JM, Cohn SL, Mattay KM *et al*. (2013). Children's Oncology Group's 2013 blueprint for research: neuroblastoma. Pediatr Blood Cancer 60: 985–993.

Pawson AJ, Sharman JL, Benson HE, Faccenda E, Alexander SP, Buneman OP *et al*. (2014). The IUPHAR/BPS Guide to PHARMACOLOGY: an expert-driven knowledgebase of drug targets and their ligands. Nucl Acids Res 42 (Database Issue): D1098–106.

Pelengaris S, Khan M, Evan GI (2002). Suppression of Myc-induced apoptosis in beta cells exposes multiple oncogenic properties of Myc and triggers carcinogenic progression. Cell 109: 321–334.

Pession A, Tonelli R (2005). The MYCN oncogene as a specific and selective drug target for peripheral and central nervous system tumors. Curr Cancer Drug Targets 5: 273–283.

Peverali FA, Orioli D, Tonon L, Ciana P, Bunone G, Negri M *et al*. (1996). Retinoic acid-induced growth arrest and differentiation of neuroblastoma cells are counteracted by N-myc and enhanced by max overexpressions. Oncogene 12: 457–462.

Reynolds CP (2000). Differentiating agents in pediatric malignancies: retinoids in neuroblastoma. Curr Oncol Rep 2: 511–518.

Reynolds CP, Kane DJ, Einhorn PA, Matthay KK, Crouse VL, Wilbur JR *et al*. (1991). Response of neuroblastoma to retinoic acid in vitro and in vivo. Prog Clin Biol Res 366: 203–211.

Reynolds CP, Schindler PF, Jones DM, Gentile JL, Proffitt RT, Einhorn PA (1994). Comparison of 13-cis-retinoic acid to trans-retinoic acid using human neuroblastoma cell lines. Prog Clin Biol Res 385: 237–244.

Reynolds CP, Matthay KK, Villablanca JG, Maurer BJ (2003). Retinoid therapy of high-risk neuroblastoma. Cancer Lett 197: 185–192.

Rubin GM, Tozer TN (1986). Hepatic binding and Michaelis-Menten metabolism of drugs. J Pharm Sci 75: 660–663.

Schug TT, Berry DC, Shaw NS, Travis SN, Noy N (2007). Opposing effects of retinoic acid on cell growth result from alternate activation of two different nuclear receptors. Cell 129: 723–733.

Seeger RC, Reynolds CP (1991). Treatment of high-risk solid tumors of childhood with intensive therapy and autologous bone marrow transplantation. Pediatr Clin North Am 38: 393–424.

Sidell N (1982). Retinoic acid-induced growth inhibition and morphologic differentiation of human neuroblastoma cells in vitro. J Natl Cancer Inst 68: 589–596.

Sidell N, Altman A, Haussler MR, Seeger RC (1983). Effects of retinoic acid (RA) on the growth and phenotypic expression of several human neuroblastoma cell lines. Exp Cell Res 148: 21–30.

Thiele CJ, Reynolds CP, Israel MA (1985). Decreased expression of N-myc precedes retinoic acid-induced morphological differentiation of human neuroblastoma. Nature 313: 404–406.

Veal GJ, Cole M, Errington J, Pearson AD, Foot AB, Whyman G *et al*. (2007). Pharmacokinetics and metabolism of 13-cis-retinoic acid (isotretinoin) in children with high-risk neuroblastoma – a study of the United Kingdom Children's Cancer Study Group. Br J Cancer 96: 424–431.

Veal GJ, Errington J, Rowbotham SE, Illingworth NA, Malik G, Cole M *et al*. (2013). Adaptive dosing approaches to the individualization of 13-cis-retinoic acid (isotretinoin) treatment for children with high-risk neuroblastoma. Clin Cancer Res 19: 469–479.

Villablanca JG, Khan AA, Avramis VI, Seeger RC, Matthay KK, Ramsay NK *et al*. (1995). Phase I trial of 13-cis-retinoic acid in children with neuroblastoma following bone marrow transplantation. J Clin Oncol 13: 894–901.

Wuarin L, Chang B, Wada R, Sidell N (1994). Retinoic acid up-regulates nuclear retinoic acid receptor-alpha expression in human neuroblastoma cells. Int J Cancer 56: 840–845.

Yu AL, Gilman AL, Ozkaynak MF, London WB, Kreissman SG, Chen HX *et al*. (2010). Anti-GD2 antibody with GM-CSF, interleukin-2, and isotretinoin for neuroblastoma. N Engl J Med 363: 1324–1334.

Supporting information

Additional Supporting Information may be found in the online version of this article at the publisher's web-site:

http://dx.doi.org/10.1111/bph.12846

Figure S1 Representative mass spectra of 13-cRA metabolites in plasma samples of patients treated with 13-cRA. The spectra shown are screen-captured images of 13-cRA metabolites detected via EPI of information-dependent acquisition (IDA). (A) m/z 315 show two different fragmentation patterns. One with retention time of 8.2 min (top) was identified as 4-oxo-13-cRA and the other with retention time of 7.1 min is presumed as methylated 13-cRA. (B) Glucuronide metabolites of 13-cRA (top) and 4-oxo-13-cRA (bottom). (C) Glutathione conjugated 4-oxo-13-cRA was identified at low levels in patient plasma.

Figure S2 Kinetic profiles of 13-cRA and 4-oxo-13-cRA glucuronide formation. Enzyme kinetics were performed using HLM and HIM (four from the top on left column) or recombinant UGT isoenzymes: UGT2B4 (bottom left) and UGT1A (middle and right column: UGT1A1, UGT1A3, UGT1A7, UGT1A8 and UGT1A9). Data are shown as the mean ± SD of $n = 3$. The substrate concentration range for the initial experiments was 0–100 μM for both 13-cRA and 4-oxo-13-cRA. In an attempt to define enzyme kinetic parameters (V_{max} and K_m), an extended range of concentration (up to 200 μM) was employed for 4-oxo-13-cRA glucuronidation as the product formation did not reach plateau within the initial range of concentrations. UGT2B7, UGT2B15 and UGT2B17 were also used for glucuronidation reaction, and 13-cRA glucuronide product was not observed with these enzymes. 4-oxo-13-cRA glucuronide were detected with all UGT2B enzymes but the glucuronide product was not detected at <50 μM of substrate with all UGT2B enzymes with UGT2B4 being the representative of other UGT2B isoenzymes (bottom left).

Table S1 Primers and probes used to detect mRNA expression.